Vietnam Journal of Earth Sciences, 46(4), 553-569, https://doi.org/10.15625/2615-9783/21368

Vietnam Journal of Earth Sciences
https://vjs.ac.vn/index.php/jse

Occurrence rate of equatorial Spread F and GPS ROTI in the ionospheric anomaly region over Vietnam

Hong Pham Thi Thu[1,2*], Christine Amory Mazaudier[3], Minh Le Huy[1,2], Susumu Saito[4], Dung Nguyen Thanh[1,2], Ngoc Luong Thi[1], Hung Luu Viet[5], Thang Nguyen Chien[1], Thanh Nguyen Ha[1], Michi Nishioka[6], Septi Perwitasari[6]

[1]*Institute of Geophysics, VAST, Hanoi, Vietnam*
[2]*Graduate University of Science and Technology, VAST, Hanoi, Vietnam*
[3]*Sorbonne Universités, UPMC Univ. Paris 06, Paris, France*
[4]*Electronic Navigation Research Institute, MPAT, Tokyo 182-0012, Japan*
[5]*Ho Chi Minh City University of Technology and Education, Ho Chi Minh City, Vietnam*
[6]*National Institute of Information and Communications Technology, Tokyo, 184-8795, Japan*

Received 30 May 2024; Received in revised form 08 July 2024; Accepted 19 August 2024

ABSTRACT

This paper presents the first observations of the occurrence rates of Spread F and GPS total electron content (TEC) index (ROTI) over Vietnam at the equatorial trough and the northern tropical crest of ionization anomaly in the Asian sector. The data have been examined for the monthly and nighttime variations in the occurrence of these two data at Bac Lieu (9.28°N, 105.73°E, dip: 1.73°N) and Phu Thuy (21.03°N, 105.95°E, dip: 14.49°N) during 2023. For Bac Lieu, the monthly variation in the occurrence of the range Spread F (RSF) has the maxima in the February, May, and September months, while the mixed Spread-F (MSF) and ROTI occurrences exhibit a semiannual asymmetry with peaks in March/April and October. For the nighttime variation, occurrence peaks at 1915-1930 LT for RSF, at about 1945-2100 LT for MSF, and between 2030-2330 LT for ROTI. Regarding the frequency Spread F (FSF) occurrence, the maximum values in the monthly variation are in April, and the nighttime variation peaks at about 2115-2315 LT. For Phu Thuy, the monthly variation of RSF, MSF, and ROTI occurrences also exhibit a semiannual asymmetry with peaks in March/April and October. These peak magnitudes are largest for ROTI, moderate for MSF, and smallest for RSF. The nighttime variation of RSF, MSF, and ROTI occurrence peaks show intense season changes from winter to autumn at pre-midnight, spring at post-midnight, and summer at post-midnight. The FSF occurrences are more significant in summer than in other seasons, mainly after midnight. The time order appearance of the Spread F types at Bac Lieu and Phu Thuy is first of RSF, then MSF, and finally FSF. This could reflect that the formation mechanisms of Spread F types are different and require further research. Our observations also showed that the post-midnight occurrence of Spread F is much larger than ROTI at Bac Lieu and Phu Thuy. The monthly variations in occurrence rates of Spread F and ROTI at Bac Lieu and Phu Thuy are similar, but these occurrence rates at Bac Lieu are usually larger than at Phu Thuy.

Keywords: Equatorial ionosphere, ionospheric irregularities, Spread F, ROTI.

1. Introduction

Due to density gradients, ionospheric irregularities are widespread at low latitudes and near the magnetic equator. These irregularities, occurring mainly in the evening and nighttime, produce rapid changes in the amplitude and phase of radio signals passing through them. These irregularities have

*Corresponding author, Email: phamhongigp@gmail.com

different sizes, from a few centimeters to a few kilometers (Kelley, 2009), affecting electromagnetic waves depending on their frequency. The Equatorial plasma Bubbles (EPB) are significant irregularities over several kilometers, while Equatorial Spread F (ESF) correspond to more minor irregularities of the order of a few decameters or less. These plasma irregularities are studied with many types of tools such as ionosonde (Equatorial Spread F), VHF/UHF radar (plumes), GPS (Scintillations), backscatter radar, and all-sky images (EPB), etc. Many studies were made on the basic plasma processes governing the generation and growth of the equatorial plasma bubble and ionospheric irregularities in the Equatorial Ionization Anomaly (EIA) region near the crest region and the magnetic equator. Many workers have been carried since the beginning of the 1970s, such as Basu and Kelley (1979), Aarons et al. (1980), Alfonsi et al. (2013) in the American sector; Das Gupta et al. (1981), Chakraborty et al. (1999), Chandra et al. (2003), Dabas et al. (2007) in the Indian sector; Huang (1970), Huang (1985), Huang et al. (1987) in the western Pacific sector; Mullen et al. (1985), Chandra et al. (2003), D'ujanga et al. (2018) in the Brazilian and African sectors; Paul et al., 2024 in the European; Lee et al. (2009), Zhang et al. (2015) in Asian sector. However, studies on the occurrence of ionospheric irregularity, and in particular, quantitative assessment of the difference in the occurrence of ionospheric irregularity in the equatorial region and the EIA crest region using simultaneously GNSS data and ionosonde data in Vietnam have not been conducted.

This study is the first attempt to compare the ROTI and the Equatorial spread F in two observatories of Vietnam: (1) Phu Thuy observatory (21.03°N, 105.96°E, dip: 14.49°N) located on the Northern crest of the EIA and (2) Bac Lieu (9.28°N, 105.73°E, dip: 1.73°N) located near the equatorial trough of the EIA. Each observatory has an ionosonde and a GNSS station. We used Equatorial Spread F derived from ionosonde data and ROTI derived from GPS TEC measurements during 2023 of the ascending phase of solar cycle 25. The remaining sections of the present paper are organized as follows: Section 2 introduces the data analyzed in the study. The results of the investigation are illustrated in Section 3. Section 4 discusses our results. Conclusions and recommendations are described in Section 5.

2. Data analysis

Table 1 shows the geographic coordinates and dip latitudes of the ionosondes and GNSS receivers at Bac Lieu and Phu Thuy. Figure 1 shows the map of Vietnam with the two observatories.

Table 1. Geographic coordinates and dip latitude of the ionospheric observatories in Vietnam

Observatory	Geographic		Dip latitude (°N)
	Latitude (°E)	Longitude (°N)	
Phu Thuy	21.03	105.96	14.49
Bac Lieu	9.28	105.73	1.73

A Digital SKI02098-Japanese ionospheric vertical sounder continuously recorded the ionosonde data at Bac Lieu. The data of the Digital SKI02098-Japanese are available on the website https://seg-web.nict.go.jp/sealion/. The ionospheric vertical sounder AIS-INGV-Italy obtained the ionosonde data at Phu Thuy (Zuccheretti et al., 2003).

The observed Equatorial Spread F (ESF) observed at Bac Lieu and Phu Thuy during 2023 are classified into four types based on the shape of diffusion on the ionogram (Fig. 2): a) frequency Spread F (FSF), b) range Spread F (RSF), c) mixed Spread F (MSF), and d) branch Spread F (BSF) (e.g., Davies, 1990). FSF is associated with narrow spectrum irregularities near the F2 peak. The FSF shows a spread near the critical frequency, typically greater than 0.3 MHz (Fig. 2a). RSF is related to fluctuations near the F2 bottom. Traces of

RSF are typically away from the critical frequency, showing a broadening in range, and are capable of exceeding 30 km in virtual height (Fig. 2b). MSF is a combination of FSF and RSF (Fig. 2c). BSF is characterized by multiple traces of similar strength, giving two or more foF_2, with the individual frequencies being well defined (Fig. 2d). The type of Spread F is scaled by manual works from the observed ionogram with a 15-min interval.

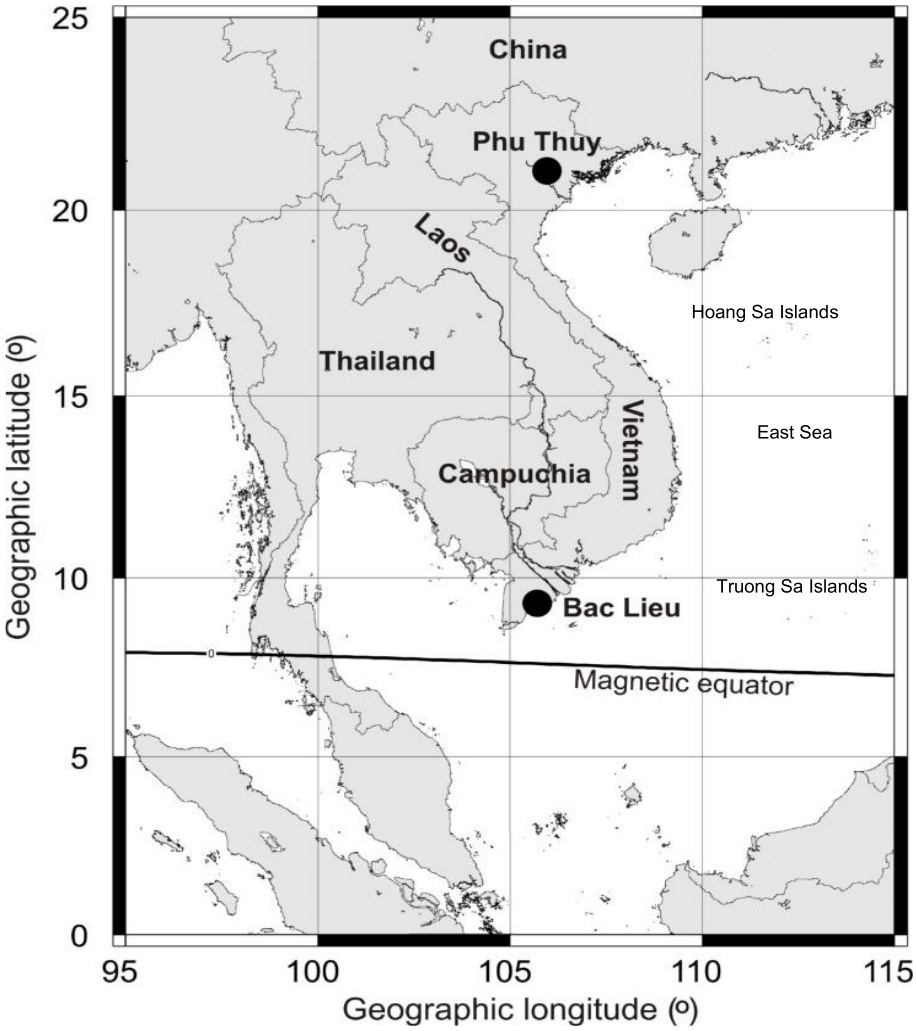

Figure 1. Ionospheric observatories at Bac Lieu and Phu Thuy

At Bac Lieu, a Septentrio PolaRx5S receiver has been installed by the National Institute of Information and Communications Technology (NICT). At Phu Thuy, a Trimble NetR9 receiver was installed by the Electronic Navigation Research Institute (ENRI) and the National Institute of Maritime, Port, and Aviation Technology. The 30-second sampling rates of two receivers are used in this study. Ionospheric irregularities cause phase and amplitude fluctuations in received GNSS signals. Phase fluctuations of the GNSS signal observed along the signal path from the satellite correspond to TEC fluctuations in the ionosphere. TEC fluctuations are characterized by a TEC rate

of change index (ROTI) based on the standard deviation of the rate of change of total electronic content (ROT) over 5 minutes to monitor ionospheric irregularities. The rate of change of slant total electron content values (ROT) is calculated by (Pi et al., 1997 Carrano and Groves, 2007; Dao et al., 2020; Nguyen Thanh et al., 2021):

$$ROT = \frac{sTEC_{\phi}(t+\delta t) - sTEC_{\phi}}{\delta t} \qquad (1)$$

where δt = 30s, and ROT in TECU/min.

$$ROTI = \sqrt{\langle ROT^2 \rangle - \langle ROT \rangle^2} \qquad (2)$$

where <> is the ensemble average values, ROTI in TECU/min.

The possible jumps in the sTEC values estimated from the carrier-phase measurements due to cycle slips were eliminated by comparing them against the sTEC estimated from the pseudo-range measurements that were smoothed by a fourth-degree polynomial approximation (Le Huy et al., 2016; Dao et al., 2020). A change in the carrier-phase sTEC of more than 5 TECU was taken to indicate a data jump. In such instances, the change in the carrier-phase sTEC was substituted by the change in the smoothed pseudo-range sTEC.

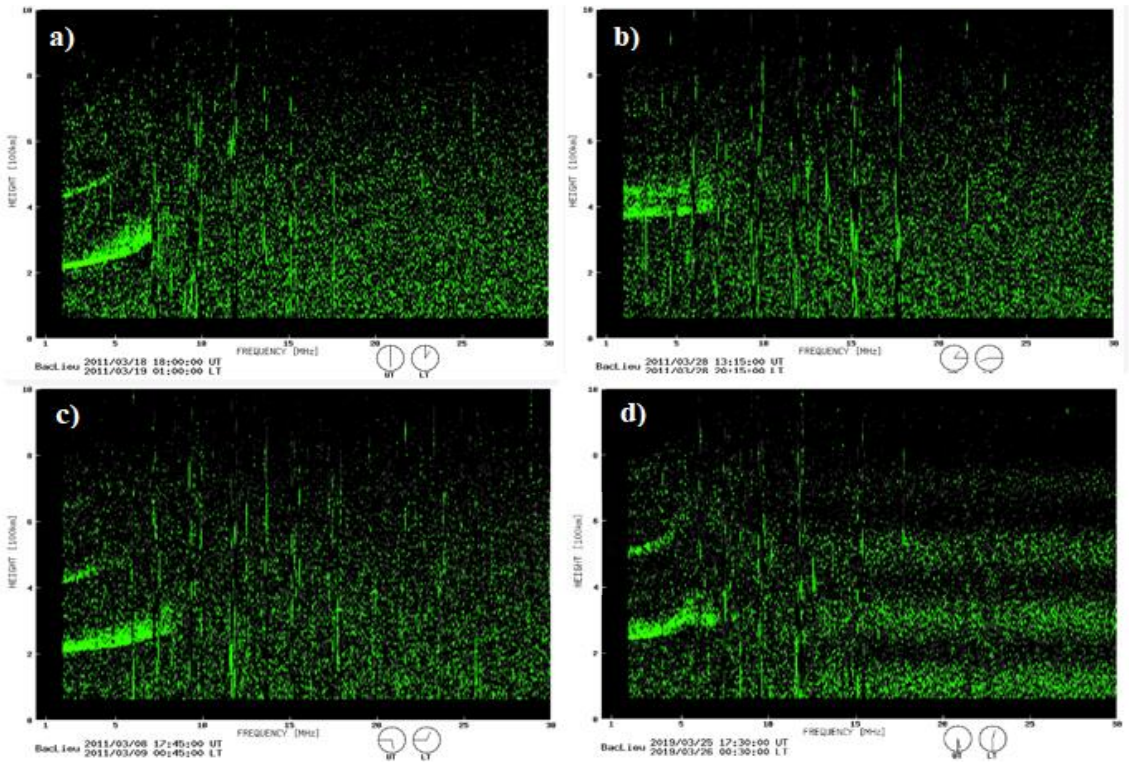

Figure 2. Ionograms with the frequency Spread F (a), the range Spread F (b), the mixed Spread-F (c), and the branch Spread F (d)

Figure 3 shows the calculated ROTI at Bac Lieu (a and b) and Phu Thuy (c and d) on 27 September 2023 (a and c) - day with scintillations and 28 September 2023 (b and d) - day without scintillations.

To reduce multipath effect, the threshold of ROTI ≥ 0.5 TECU/min and satellite elevation angle $\alpha \geq 30^{o}$ are used to determine ionospheric irregularity day (Nguyen Thanh et al., 2021).

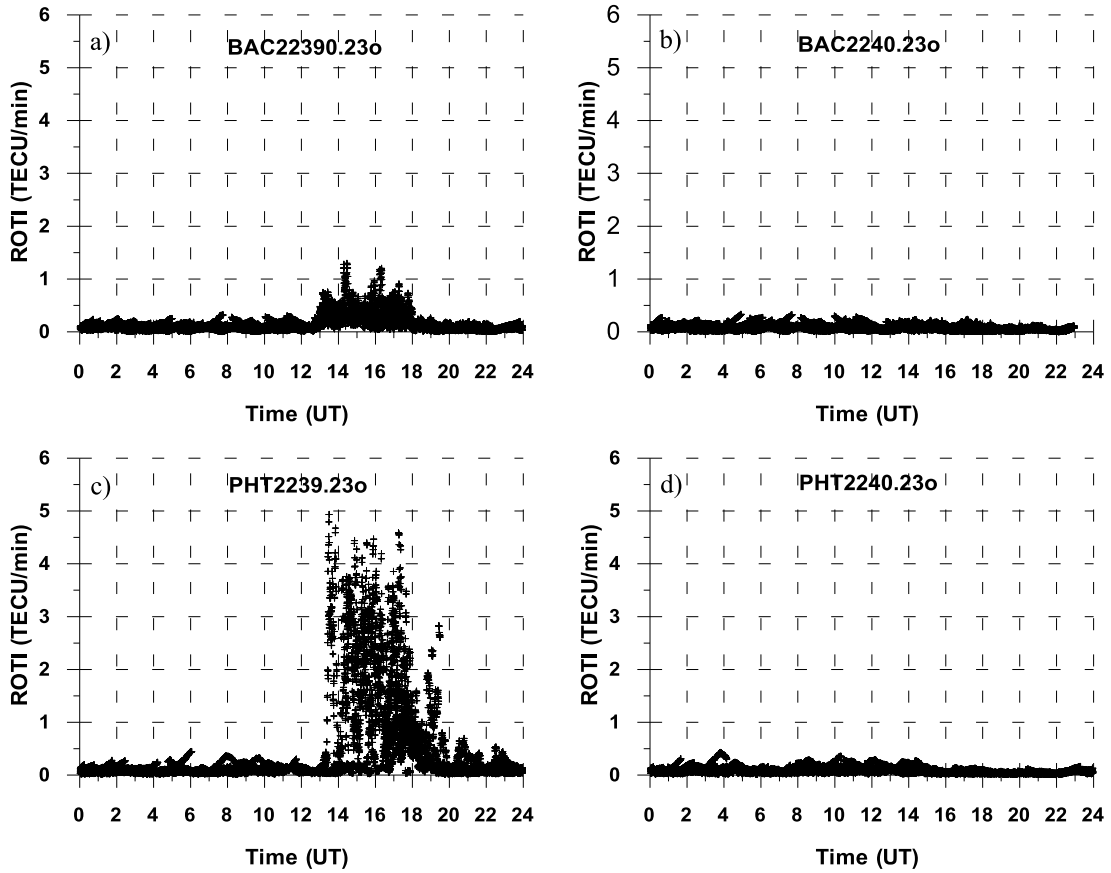

Figure 3. ROTI at Bac Lieu (a and b) and Phu Thuy (c and d) on 27 September 2023 (day 239) and on 28 September 2023 (day 240)

The occurrence rates of Spread F/ROTI are calculated according to the following:

$$R = \frac{N_S}{N} * 100\% \quad (3)$$

N_S denotes the total number of epochs where the ESF/ionospheric scintillation index is above the threshold within a certain period; N is the total number of epochs within a certain period.

This monthly variation in occurrence is the percentage of days at least one spread F/ROTI event is observed daily in one month.

The occurrence rate is the number of spread F/ROTI events in an hour divided by the total number of observed ionograms/total number of epochs where the ROTI is above the given threshold within one hour for a season.

The seasonal variation is grouped into four seasons: Spring (March, April), summer (May, June, July, August), autumn (September, October), and winter (November, December, January, and February).

3. Results

3.1. Occurrence rates of Spread F and ROTI at Bac Lieu

Figure 4 depicts monthly variations in occurrence rates of Spread F and enhanced ROTI during 1800-0000 LT (Fig. 4a), 0000-0600 LT (Fig. 4b), and 1800-0600 LT (Fig. 4c) with the black line showing all Spread F types for each period during 2023 at Bac Lieu.

In Fig. 4a during 1800-0000 LT (pre-midnight), the RSF occurrence has three peaks in May (14.69%), February (12.27%)

and December (13.41%); the FSF occurrence peaks in April (17.75%); while the MSF occurrence has two peaks, the first peak ranges from February to April (28%-35%), the second peak is in October (48.28%); ROTI has two peaks in March (43.65%) and October (33.57%). In Fig. 4b during 0000-0600 LT (post-midnight), the RSF, FSF, MSF and ROTI occurrence the first peak in April (5.72%, 18.07%, 19.43%, 9.19%, respectively), the second peak occurrences in August for MFS (20.64%), ROTI (6.53%), while this second peak occurrences in October for RFS (7.87%), September for FSF (6.28%). In Fig. 4c during the whole night (1800-0600 LT), RFS occurrences are maxima in February (8.72%), May (8.41%), and October (9.56%); For FSF occurrence, the maximum occurrence is in April (17.92%); The MSF and ROTI occurrences are maxima in the equinoctial months and minima in the solstice months.

Generally, the monthly average variations in Spread F types at Bac Lieu exhibit a semiannual variation, with the first maximum in March/April and the second maximum in September/October for each period as ROTI. There are exceptions for RFS and FSF during 1800-0000 LT. RSF and FSF show nearly annual variation, with the maximum in April for RFS and May for FSF. These monthly variations of Spread F and ROTI appear strong pre-midnight and weak post-midnight. MSF occurrence appears more dominant than RFS and FSF for each period.

Figure 5 presents the seasonal variations in the occurrence of Spread F and ROTI at Bac Lieu for each season, for spring (left top panel), autumn (left bottom panel), summer (right top panel), and winter (right bottom panel). On each panel, the colored curves correspond to the different Spread F and the black line to all the Spread F types.

In Fig. 5a for spring, the seasonal variation of RSF occurrence peaks at 1915 LT (36.00%), then decreases sharply. The MSF occurrence increases at 1915 LT, peaks at 2015 LT (58.00%), and decreases gradually. The FSF occurrence increases from 1915 to 2245 LT, reaches a maximum (34.61%) at this time, then keeps a value of 23.52%-32% until 0015 LT, and decreases gradually. The variation of ROTI occurrence is similar to MSF occurrence and peaks at 2130 LT (54.49%). For the BSF, occurrence appears very weak.

In Fig. 5b for summer, the RSF occurrence peaks at 1930 LT (21.55%); this peak continued to fluctuate during 2 hours with values from 18.01% to 21.55%, then decreases to 0100 LT and reaches three more small peaks at 0115, 0415, 0530 LT, respectively. The maximum FSF occurrence is less than 7.76% at 2115 LT. The MSF and ROTI occurrences increase gradually from 1900 LT and maintain a maximum at 2245 LT (29.66%) and 2330 LT (15.44%), respectively. The BSF occurrence was almost absent.

In Fig. 5c for autumn, the RSF occurrence peaks at 1915 LT (25.93%), then decreases and attaints a peak at 0230 LT (25.93%). The MSF occurrence peaks at 1945 LT (61.11%) and then decreases gradually. The FSF occurrence obtains the first maximum at 2300 LT (11.32%) and then reaches the second maximum at 0345 LT (12.73%). Its maximum is maintained during two hours (12.73-12.96%) and decreases gradually. The ROTI peak occurs at 2030 LT, one hour later than MSF. In general, the variation of MSF has the same morphology as ROTI. The BFS occurrence is not almost present.

During winter (Fig. 5d), the RSF occurrence peaks at 1915 LT (35.29%) and then decreases gradually, two hours earlier than MSF (maximum at 2100 LT (46.21%)) and ROTI (maximum at 2130 LT (12.84%)), three hours earlier than FSF (peak at 2230 LT (20.69%)). The BSF occurrence is infrequent.

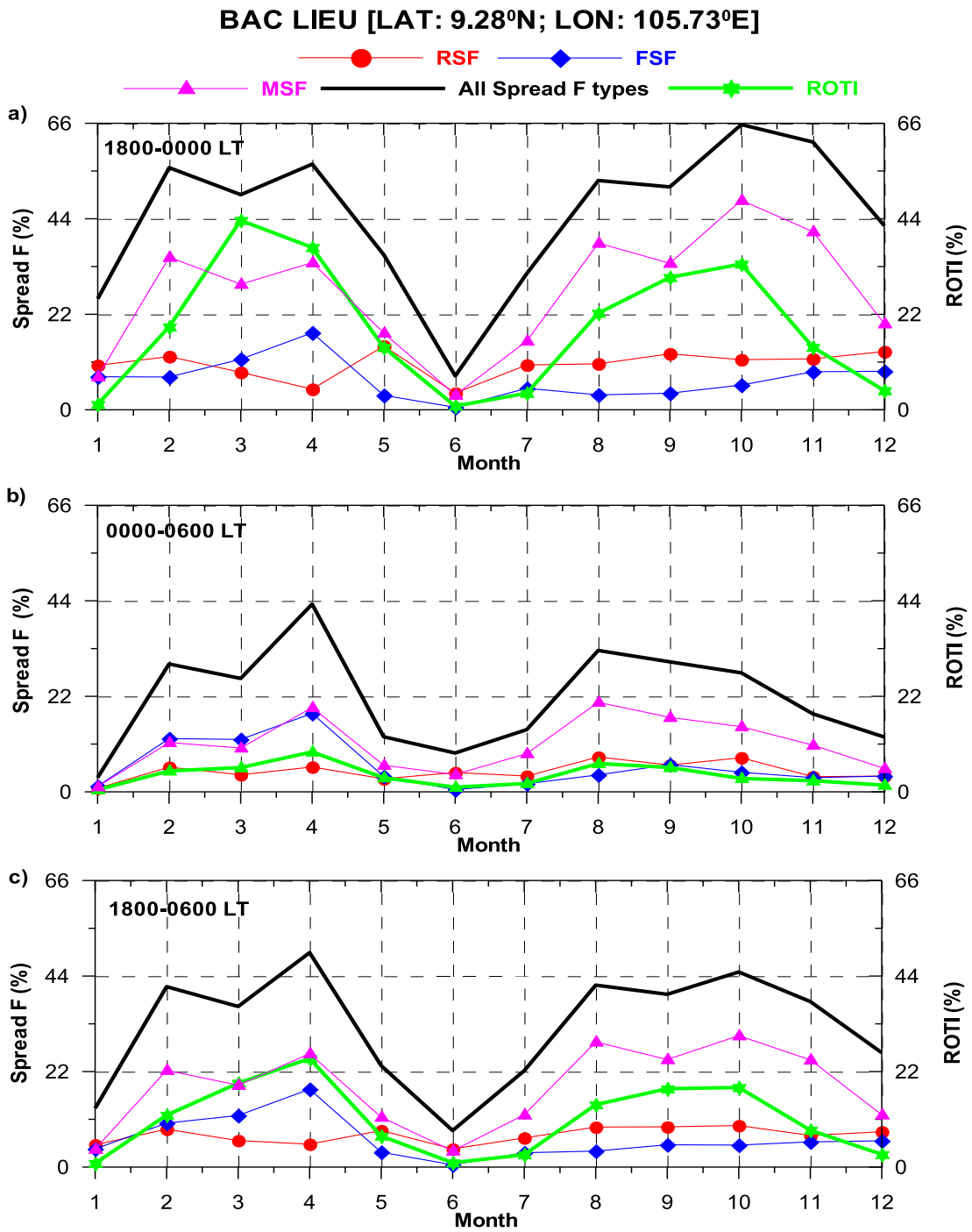

Figure 4. Monthly variations in occurrence rates of RSF (red circle), FSF (blue diamond), MSF (pink triangle), and ROTI (green star) during 1800-000 (a), 0000-0600 (b), 1800-0600 LT (c) during 2023 at Bac Lieu station. The black solid line on each plot is those of all Spread F types for each corresponding period

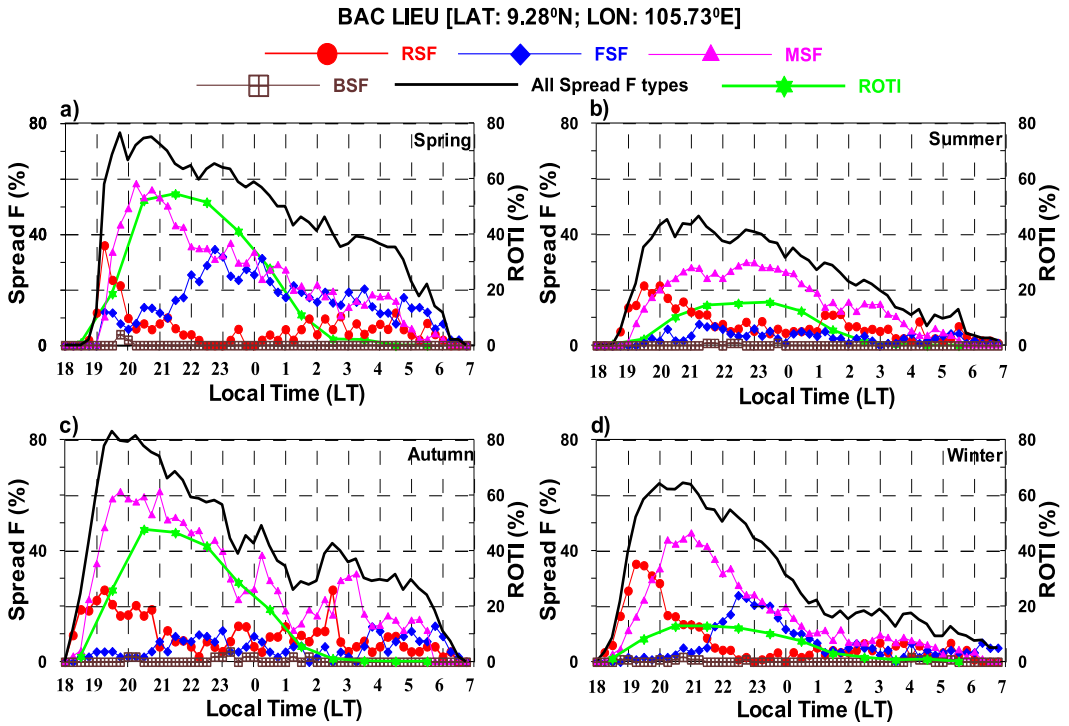

Figure 5. Nighttime seasonal variation of monthly mean values of occurrence rates of RSF (red circle), FSF (blue diamond), MSF (pink triangle), BSF (brown square), and ROTI (green star) during 2023 at Bac Lieu station. The black solid line on each plot shows the local time variation of occurrence rates for all Spread F types for each corresponding season

In general, the nighttime variations of Spread F occurrence are similar to those of ROTI, mainly before midnight, while Spread F occurs larger than ROTI after midnight. Besides, Spread F and ROTI appear dominant in the equinox months compared to summer and winter. The times of appearance of Spread F types are first RSF, followed by MSF and FSF. RSF always appears about one to two hours earlier than ROTI. The characteristics of RSF and FSF at Bac Lieu are also consistent with Hoang Thai Lan et al. (2011) results. In Vietnam, Hoang Thai Lan et al. (2011) studied Spread F's characteristics based on the ionograms obtained at Ho Chi Minh City (10.5°N, 106.33°E, magnetic latitude: 2.9°N) for 2003. They have found that RSF occurred pre-midnight (2100-2200 LT) and appeared more in February, March, and April, while FSF occurred post-midnight (2300-0100LT) and showed maximum occurrence during equinox months.

3.2. Occurrence Rates of Spread F and ROTI at Phu Thuy

Figure 6 presents the monthly variations in Spread F and ROTI occurrence rates at Phu Thuy for the three periods during 2023.

In Fig. 6a for 1800-0000 LT, the RSF peak, MSF peak, and ROTI peak amplitudes show clearly a semiannual variation with the first maximum in March/April (4.26%, 8.17%, 22.74%, respectively), the second maximum in October (7.48%, 11.28%, 30.63%, respectively), and two minima in solstices. Figure 6a also presents an equinoctial asymmetry with the RSF, MSF, and ROTI peak amplitudes more extensive in March/April than in October: the spring maximum is smaller than the autumnal one.

The FSF occurrence exhibits an annual variation with the highest values in July (2.92%) and minima in winter. In Fig. 6b for 0000-0600 LT, the RSF, MSF, and ROTI occurrences have two maximum values in April (6.17 %, 10.15%, 11.78%, respectively). August/November (4.61%, 6.04%, 9.09%, respectively), with the first maximum being more significant than the second one, while the FSF occurrence has a maximum in June. For the whole night (1800-0600 LT) (Fig. 6c), the RSF, MSF, and ROTI have more extraordinary occurrences in April (5.25%, 8.94%, 15.85%, respectively) and October (5.10%, 7.15%, 17.23%, respectively). The more extraordinary occurrences of FSF are generally found in June (7.33%). In general, the Spead F and ROTI occurrences are more significant in pre-midnight than post-midnight, except FSF, when its occurrence is greatest post-midnight.

Figure 7 presents the seasonal variations in the occurrence of Spread F and ROTI for 2023 at Phu Thuy for the four seasons.

In Fig. 7a for spring, the RSF starts to appear from 1945 LT, increases gradually to 0000 LT, attaints a maximum at 0030 LT (15.79%), and then decreases gradually. For MSF, the occurrence starts from 1930 to 2015. LT reaches a value of approximately 14.04%; this value maintains until 0115 LT, then reaches a maximum at 0130 LT (19.64%) and decreases gradually. The occurrence of FSF increases rapidly from 0115 to 0200 LT and reaches its maximum at 0300 LT (12.24%). A peak of ROTI occurrence appears at 2130 LT (31.89%); this maximum value fluctuates for 3 hours, then decreases gradually. In general, the appearance time of Spread F types is about four or six hours later than that of ROTI.

In Fig. 7b, the RFS maximum occurrence is less than 6% during the summer months at 0145 LT. The amplitude of the MSF peak fluctuates around 5.21% between 2130 and 0300LT, reaching a maximum at 0345 LT (7.69%). The FSF occurrence increases gradually from 2115 LT and reaches its maximum value at 0430 LT (21.84%), then decreases gradually. The occurrence of ROTI is almost found around midnight with a maximum value of 8.39% at 0030 LT, one hour/three hours/four hours earlier than RSF, MSF, and FSF, respectively. Furthermore, the variations in the occurrence of FSF are more significant than those of RSF and MSF.

During the autumn (Fig. 7c), the maxima occurrences of RSF and ROTI appear at almost the same time at about 2130 LT (with values of 12.96% and 34.53%, respectively), while the maximum of MSF appears at 2215 LT (18.18%), one hour after in comparison to RSF and ROTI. The occurrence value reaches its maximum at 0330 LT (7.41%) for the FSF.

In Fig. 7d for winter, the occurrences of Spread F types are less than 7%. The peak times of occurrences are at 2045 LT for RSF and 0545 LT for FSF, while the peak times of MSF are before midnight (2100 LT) and after midnight (0015 LT). The occurrence of ROTI presents a maximum at 2130 LT (15.73%), then decreases rapidly.

Spread F in Phu Thuy appears mainly during the equinox, except for FSF, which appears strongly in the summer compared to other seasons. Figure 7 also shows that the average seasonal variations in Spread F and ROTI occurrence are different for the four seasons, except for RSF and MSF in summer, autumn, and winter, which are somewhat similar to ROTI. These results indicate that the characteristics of Spread F in Phu Thuy may not be entirely related to ROTI, although ROTI is related to RSF MSF. These results observed in Phu Thuy are consistent with the previous studies (Huang, 1970; Huang et al., 1987; Lee et al., 2009). In addition, our observations show that the appearance time of Spread F types at Phu Thuy for RSF, MSF, and FSF are similar to the observations in Bac Lieu, but Spread F at Phu Thuy

frequently occurs after ROTI. The occurrence rate of ROTI dominated at pre-midnight in this paper is similar to that obtained by Tran et al. (2017).

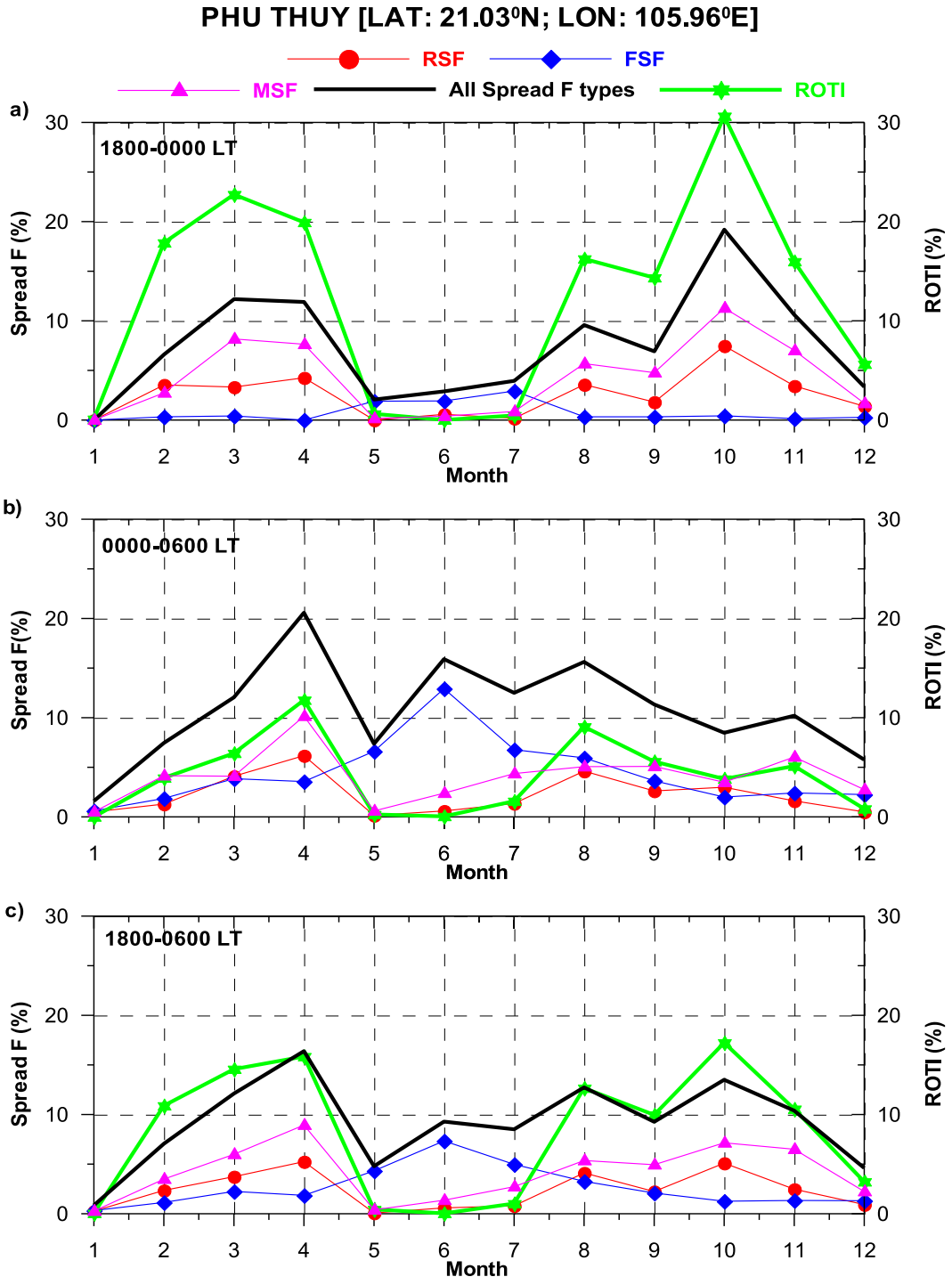

Figure 6. The figure is similar to Fig. 4 for Phu Thuy

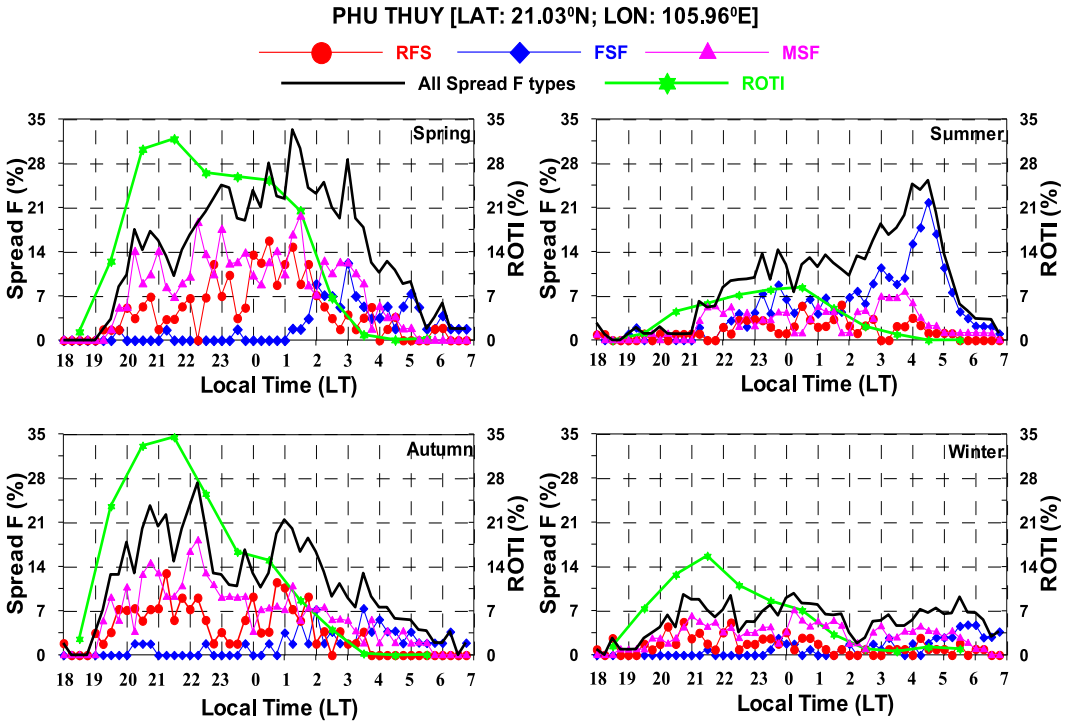

Figure 7. The figure is similar to Fig. 5 for Phu Thuy

4. Discussions

At Bac Lieu, the monthly variations in MSF and ROTI occurrence rates (in Fig. 4) are similar but not wholly consistent with those of RSF and FSF. This discrepancy could be caused by the different formation mechanisms of Spread F types, but the formation mechanisms of MSF and ROTI are similar.

Figure 5 shows that Spread F and ROTI percentages are different, but their time variation is similar; this can be due to different measurement methods. The Spread F and ROTI occur mainly before midnight. Still, the nighttime occurrence rates of ROTI (in Fig. 5) are lower than those of Spread F. According to Ma & Maruyama (2006), Alfonsi et al. (2011), and Yang & Liu (2016), the irregularity size for ROTI is a few kilometers, while spread F observed on ionogram is caused by irregularities of decameter scale size or less. In addition, Rodrigues et al. (2004) and Chen et al. (2006) explained that the scale sizes of irregularities forming Spread F and ROTI are different, and these discrepancies might be ascribed to the smaller altitudinal distribution of irregularities, which is not capable of fluctuating GPS signals, but could be detected by an ionosonde.

The magnetic field is horizontal at the magnetic equator, and this geometric property is the origin of the Equatorial Ionization Anomaly (EIA). At low altitudes, the dominant Lorentz force imposes an electrical drift ExB on the plasma in the E region, and an Eastward/Westward electric field lifts/down the ionospheric plasma. At higher altitudes in region F, gravity and pressure gradient forces cause plasma diffusion along the magnetic field lines and form the EIA with a trough of density at the equator and two density peaks at 15°N/S. The eastward electric field during the day increases sharply before becoming westward post-sunset; this is the

pre-reversal enhancement (PRE) (Kelley, 2009). The magnitude of the upward ExB drift velocity of pre-reversal enhancement (PRE) plays a dominant role in the variability of F region irregularities. The faster the PRE upward velocity is, the more significant the growth rate of Rayleigh-Taylor instability is (Fejer et al., 1999; Lee et al., 2005a, 2005b; Lee, 2006). Hong et al. (2022) found that the magnitude of PRE upward velocity at Bac Lieu is more significant in the equinox months than in the solstice months. This explains why ROTI and Spread F occurrence at Bac Lieu have two peaks in April and October.

At Phu Thuy, Fig. 6 shows that the monthly variations in RSF, MSF, and ROTI are similar and different from those of FSF. This result indicates that the RSF, MSF, and ROTI have the same generation mechanism, which differs from the generation mechanism of FSF. Figure 7 shows that the ROTI occurrence is more significant than the Spread F occurrence before and minor after midnight.

It is well known that the F region irregularities often occur at the dip equator, lifted to higher altitudes, and then extended to higher latitudes. Since the monthly variation in occurrence probability of RSF, MSF, and ROTI at Phu Thuy should be related to the equatorial F region irregularities, the semiannual variations of RSF, MSF, and ROTI occurrences present at Phu Thuy (in Figs. 6 and 7), which is the result of the equatorial F region irregularities. Hong et al. (2022) also showed that the PRE peak time at Bac Lieu was earlier than at Phu Thuy. This is also why Spread F at Phu Thuy peaked later than in Bac Lieu.

In addition, in the post-midnight, the occurrences of Spread F are more significant than those of ROTI at both stations (Figs. 5 and 7); this implies that the large-scale irregularities decay meanwhile the small-scale irregularities still exist, which could be due to the bifurcation of EPBs before dissolution (Yokoyama, 2017).

Next, we observed that the monthly variations in the occurrence of FSF at Phu Thuy are not similar to RSF, MSF, and ROTI (in Figs. 6 and 7). This indicates that the mechanism formation of FSF may not be related to the equatorial F region irregularities. In our study, the occurrence probability of FSF at Phu Thuy was observed to be similar to the one of Spread F at Chungli (25°N, 121.6°E; geomagnetic latitude: 14.5°N) near the EIA crest (Lee et al., 2009) and at midlatitudes in the western Pacific sector (Shiokawa et al., 2003). Thus, the formation mechanisms for FSF at Phu Thuy and Spread F at midlatitudes could be similar. At mid-latitudes, the mechanism generating the Spread F was explained by Perkins instability (Perkins, 1973; Fukao et al., 1991; Kelley and Fukao, 1991). However, the growth rate of the Perkins instability might be too low to generate any significant irregularity in the *F* region (e.g., Kelley and Fukao, 1991). Additional mechanisms to accelerate the Pekins instability are necessary as the Perkins-type MSTID (Bowman, 1990; Shiokawa et al., 2003) and E-F coupled instability (Cosgrove and Tsunoda, 2003; Haldoupis et al., 2003). All these mechanisms can generate the F region irregularities at midlatitude and Phu Thuy, but specific studies of each of these mechanisms have not yet been carried out. Therefore, further investigation of the FSF mechanisms at Phu Thuy and midlatitude is necessary.

Figure 8 shows the monthly variations in occurrence rates of Spread F (Fig. 8a) and ROTI (Fig. 8b) at Bac Lieu (red open circle) and Phu Thuy (blue solid circle) during 2023. Spread F and ROTI occurrences at Bac Lieu have maximum/minimum in equinox (April and October)/solstice (January, May, June, July, and December). This seasonal variation is also in Phu Thuy (blue solid circle in Fig. 8).

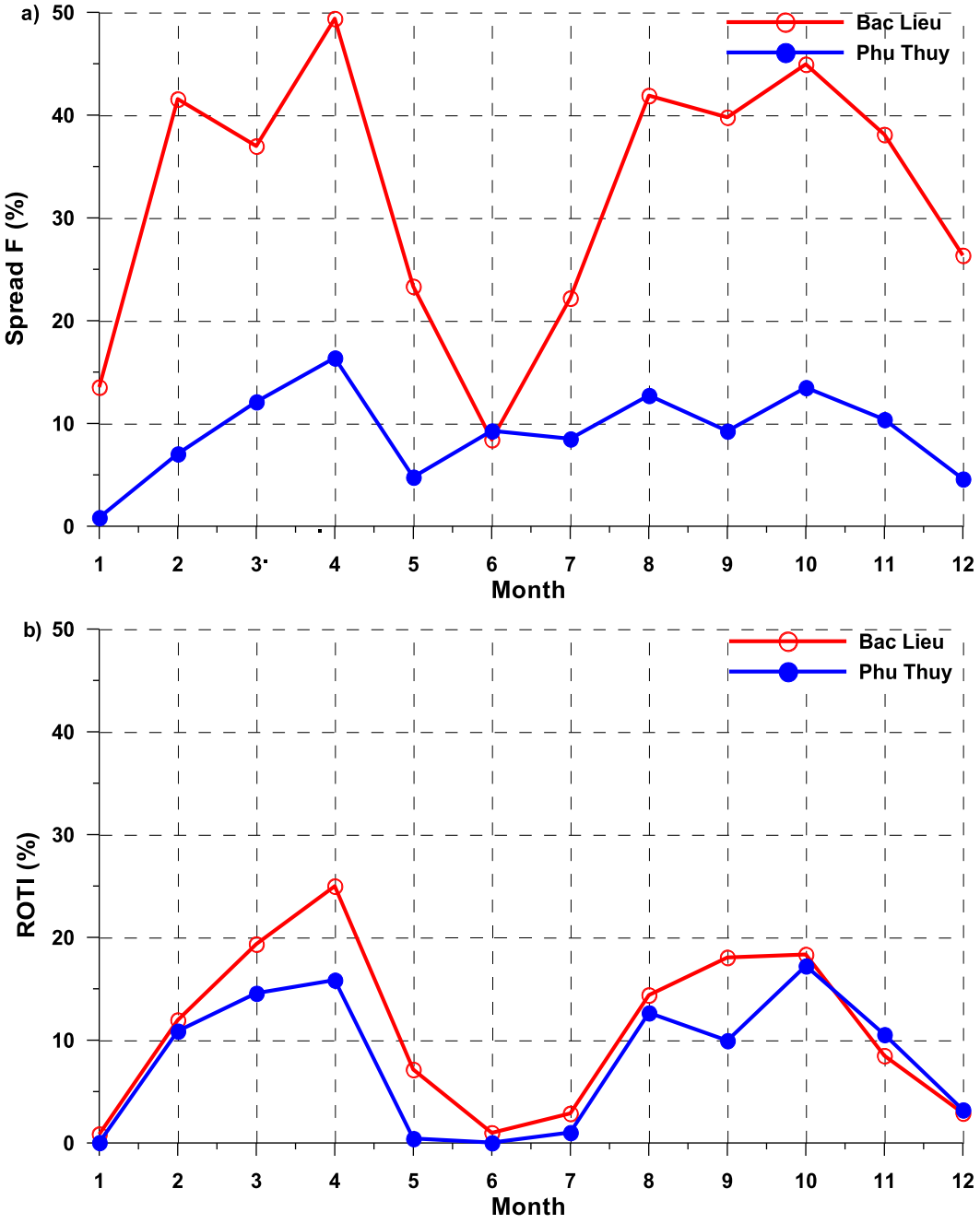

Figure 8. Monthly variations in occurrence rates of Spread F (a) and ROTI (b) at Bac Lieu (red open circle) and Phu Thuy (blue solid circle) during 2023

However, ESF occurrence at Bac Lieu is higher than at Phu Thuy. For Spread F, it should be noted that it is difficult to compare the absolute value of ESF occurrences because of different sensitivities between ionosondes at Bac Lieu and Phu Thuy. Still, the relative variation in reason can be compared. Fig. 8 also shows that Spread F and

ROTI occurrence rates at Bac Lieu are usually larger than at Phu Thuy. This could explain that not all irregularities at the equator can extend to the crest (Saito and Maruyama, 2006). The appearance of ROTI at Phu Thuy and Bac Lieu occurs mainly during equinoctial months (April and October), consistent with the previous studies in East and Southeast Asia (Tran et al., 2017; Li et al., 2021). Li et al. 2021 locate the EPBs at latitudes of +/or -25° for high solar activity conditions. Our stations Phu Thuy (21.03°E) and Bac Lieu (9.08°E) are in this range of latitudes, and the year 2023 is near the maximum of cycle 25 with a mean sunspot number more significant than 120.

By using the Spread F and the phase and amplitude scintillation index at Tucumán (26,9°S, 294,6°E, magnetic latitude 15.5°S) in Argentina (magnetic latitude similar to the one at Phu Thuy but in the southern hemisphere), Alfonsi et al. (2013) showed that the occurrence of all four types of Spread F (strong range Spread F, range Spread F, frequency Spread F and mixed Spread F) is higher in summer and lower in winter while the occurrence of scintillations peaks at equinox in post sunset sector and shows a minimum in winter. Meanwhile, at Phu Thuy, Spread F (RSF, FSF, MSF) and ROTI occurrence rates show a maximum at equinox and a minimum in winter. This indicates that Spread F and ROTI are local, and the results obtained in this study contribute to the understanding of short-term variations of ionospheric irregularities in Vietnam.

5. Conclusions

In this study, we use ionosondes and GNSS receivers at Bac Lieu and Phu Thuy during 2023, the year of the ascending phase of solar cycle 25, to investigate the F region irregularities at the equator and near the Northern crest of the EIA in Vietnam. We studied the monthly and nighttime variations in spread F and ROTI occurrence rates for the first time. The following results are drawn from the analysis.

For Bac Lieu, the monthly variation in the occurrence probability of RSF has the maxima in February, May, and September. MSF and ROTI occurrences exhibit a semiannual asymmetry with peaks in March/April and October. For the nighttime variation, occurrence probability peaks at 1915-1930 LT for RSF, at about 1945-2100 LT for MSF, and between 2030-2330 LT for ROTI. Regarding the FSF occurrence, the maximum values in the monthly variation are in April, and the nighttime variation peaks at about 2115-2315 LT. The appearance time of the Spread F types is RSF, MSF, and FSF, respectively, and RSF appears always earlier than ROTI.

For Phu Thuy, the monthly variation of RSF, MSF, and ROTI occurrences also exhibit a semiannual asymmetry with peaks in March/April and October. These peak magnitudes are largest for ROTI, moderate for MSF, and smallest for RSF. The nighttime variation of RSF, MSF, and ROTI occurrence peaks show vital season changes from winter at 2045 LT, 2100 LT, 2130 LT to autumn at 2130 LT, 2215 LT, 2130 LT, spring at 0030 LT, 0130 LT, 2130 LT, and summer at 0145 LT, 0345 LT, 0130 LT. The FSF occurrences are more significant in summer than in other seasons, mainly after midnight. The Spread F occurrence time occurs RSF, MSF, and FSF, respectively, and appears always after ROTI.

Our observations should also be that the post-midnight occurrence of Spread F is much larger than ROTI at Bac Lieu and Phu Thuy. Spread F and ROTI occurrence rates at Bac Lieu are usually larger than at Phu Thuy.

The result of the study of the F region irregularities at Bac Lieu and Phu Thuy can provide interesting characteristics of ionospheric plasma dynamics in Vietnam at the equator and near the EIA crest. In the

future, we would like to investigate further long datasets simultaneously at two stations about Spread F mechanisms, separating the characteristics in occurrence probability of irregularities during pre-midnight and post-midnight periods and separating the occurrence characteristics of irregularities related to plasma bubbles (appeared at Bac Lieu before at Phu Thuy) or MSTIDs (appeared at Phu Thuy before at Bac Lieu).

Acknowledgments

Vietnam Academy of Science and Technology funds this research under grant VAST05.03/22-23, NVCC12.02/24-24. The authors thank the NGDC data center for the basis of indices of geomagnetic activity and Earth's magnetic field components (IGRF). The Bac Lieu data are available on the website http://seg-web.nict.go.jp/sealion/.

References

Aarons J., J.P. Mullen, H.E. Whitney, E.M. Mackrnzie, 1980. The dynamics of equatorial irregularity patch formation motion and decay. J. Geophys. Res., 85, 139–149.

Alfonsi L., L. Spogli, J.R. Tong, G. De Franceschi, V. Romano, A. Bourdillon, C.N. Mitchell, 2011. GPS scintillation and TEC gradients at equatorial latitudes in April 2006. Advances in Space Research, 47(10), 1750–1757. https://doi.org/10.1016/j.asr.2010.04.020.

Alfonsi L., L. Spogli, M. Pezzopane, V. Romano, E. Zuccheretti, G. De Franceschi, M.A. Cabrera, R.G. Ezquer, 2013. Comparative analysis of spread-F signature and GPS scintillation occurrences at Tucumán, Argentina. J. Geophys. Res.: Space Physics, 118, 4483–4502. Doi: 10.1002/jgra.50378.

Basu S., M.C. Kelley, 1979. A review of recent observations of equatorial scintillations and their relationship to current theories of F region irregularity generation. Radio Science, 14, 471–485.

Bowman G.G., 1990. A review of some recent work on midlatitude spread F occurrence as detected by ionosondes. J. Geomag. Geoelectr., 42, 109–138.

Carrano C., K. Groves, 2009. Ionospheric data processing and analysis. Workshop on Satellite Navigation Science and Technology for Africa. The Abdus Salam ICTP, Trieste, Italy.

Chakraborty S.K., A. DasGupta, S. Ray, S. Banerjee, 1999. Long-term observation of VHF scintillation and total electron content near the crest of the equatorial anomaly in the Indian longitude zone. Radio Sci., 34, 241–255. Doi: 10.1029/98RS02576.

Chandra H., S. Sharma, M.A. Abdu, I.S. Batista, 2003. Spread-F at anomaly crest regions in the Indian and American longitudes. Adv. Space Res., 31, 717–727. Doi: 10.1016/S0273-1177(03)00034-6.

Chen W.S., C.C. Lee, J.Y. Liu, F.D. Chu, B.W. Reinisch, 2006. Digisonde spread F and GPS phase fluctuations observed in the equatorial ionosphere during solar maximum. J. Geophys. Res., 111, A12305. Doi: 10.1029/2006JA011688.

Cosgrove R.B., R.T. Tsunoda, 2003. Simulation of the nonlinear evolution of the sporadic E layer instability in the nighttime midlatitude ionosphere. J. Geophys. Res., 108(A7), 1283. Doi: 10.1029/2002JA009728.

Dao T., M. Le Huy, B. Carter, Q. Le, Trinh T.T., B.N. Phan, Y. Otsuka, 2020. New observations of the total electron content and ionospheric scintillations over Ho Chi Minh City. Vietnam Journal of Earth Sciences, 42(4), 320–333. Doi: 10.15625/0866-7187/42/4/15281.

Dabas R.S., Rupesh M. Das, Kavita Sharma, S.C. Garg, C.V. Devasia, K.S.V. Subbarao, K. Niranjanc, P.V.S. Rama Rao, 2007. Equatorial and low latitude spread-F irregularity characteristics over the Indian region and their prediction possibilities. J. Atmos. Sol. Terr. Phys., 69, 685–696.

Das Gupta A., A. Maritra, S. Basu, 1981. Occurrence of nighttime VHF scintillations near the equatorial anomaly crest in the Indian sector. Radio Sci., 16, 1455–1458. Doi: 10.1029/RS016i006p01455.

Davies K., 1990. Ionospheric Radio, Peter Peregrinus Ltd., London.

D'ujanga F.M., G. Lugonvu, B. Ndiny, 2018. Probing the equatorial ionosphere using spread-F signatures and GPS scintillations at Maseno in East Africa. Adv. Space Res., 62, 1753–1761.

Fejer B.G., L. Scherliess, E.R. de Paula, 1999. Effects of the vertical plasma drift velocity on the generation and evolution of equatorial spread F.

J. Geophys. Res., 104(19), 859–869. Doi: 10.1029/1999JA900271.

Fukao S., M.C. Kelley, T. Shirakawa, T. Takami, M. Yamameto, T. Tsuda, S. Kato, 1991. Turbulent upwelling of the midlatitude ionosphere: 1. Observational results by the MU radar. J. Geophys. Res., 96, 3725–3746. Doi: 10.1029/90JA02253.

Haldoupis C., M.C. Kelley, G.C. Hussey, S. Shalimov, 2003. Role of unstable sporadic E layers in the generation of midlatitude spread F. J. Geophys. Res., 108(A12), 1446. Doi: 10.1029/2003JA009956.

Hong Pham Thi Thu, Christine Amory Mazaudier, Minh Le Huy, SusumuSaito, Kornyanat Hozumi, Dung Nguyen Thanh, Ngoc Luong Thi, 2022. Nighttime morphology of vertical plasma drifts over Vietnam during different seasons and phases of sunspot cycles. Adv. Space Res., 70, 411–426. ISSN: 0273-1177. https://doi.org/10.1016/j.asr.2022.04.010.

Huang C.-M., 1970. F region irregularities that cause scintillations and spread F echoes at low-latitude. J. Geophys. Res., 75, 4833–4841. Doi: 10.1029/JA075i025p04833.

Huang Y.N., 1985. Ionospheric electron content depletion associated with amplitude scintillation at the equatorial anomaly crest zone. J. Geophys. Res., 90, 4333–4339. Doi: 10.1029/JA090iA05p04333.

Huang Y.N., K. Cheng, W. T. Huang, 1987. Seasonal and solar cycle variations of spread F at the equatorial anomaly crest zone. J. Geomag. Geoelectr., 39, 639–657.

Kelley M.C., 1989. The Earth's Ionosphere, Int. Geophys. Ser, vol. 43, Academic, San Diego, Calif.

Kelley M., 2009. The Earth's Ionosphere: Plasma Physics and Electrodynamics, 96, second ed. eBook ISBN: 9780080916576. Academic Press. Elsevier, New-York.

Paul K.S., M.H. Rafi, H. Haralambous, M.G. Mostafa, 2024. Correlation of Rate of TEC Index and Spread F over European Ionosondes. Atmosphere, 15, 331. https:// doi.org/10.3390/atmos15030331.

Lan H.T., N.T. Trang, J. Macdougall, 2011. The occurrence of equatorial spread F over Ho Chi Minh City in years 2003 and 2005. Vietnam Journal of Earth Sciences, 33(2), 126–133. https://doi.org/10.15625/0866-7187/33/2/287.

Lee C.C., 2006. Examine the local linear growth rate of collisional Rayleigh-Taylor instability during solar maximum. J. Geophys. Res., 111, A11313. Doi: 10.1029/2006JA011925.

Lee C.C., F.D. Chu, W.S. Chen, J.Y. Liu, S.-Y. Su, Y.A. Liou, S.B. Yu, 2009. Spread F, GPS phase fluctuations, and plasma bubbles near thecrest of equatorial ionization anomaly during solar maximum. J. Geophys. Res., 114, A08302. Doi: 10.1029/2009JA014195.

Lee C.C., S.-Y. Su, B.W. Reinisch, 2005a. Concurrent study of bottomside spread F and plasma bubble events in the equatorial ionosphere during solar maximum using Digisonde, and ROCSAT-1. Ann. Geophys., 23, 3473–3480.

Lee C.C., J.Y. Liu, B.W. Reinisch, W.S. Chen, F.D. Chu, 2005b. The effects of the pre-reversal ExB drift, the EIA asymmetry, and magnetic activity on the equatorial spread F during solar maximum, Ann. Geophys., 23, 745–751.

Le Huy M., L. Tran Thi, R. Fleury, C. Amory-Mazaudier, T. Le Truong, T. Nguyen Chien, T. Nguyen Ha, 2016. TEC variations and ionospheric disturbances during the magnetic storm in March 2015 observed from continuous GPS data in the Southeast Asia region. Vietnam Journal of Earth Sciences, 38(3), 267-285.

Li G., B. Ning, Y. Otsuka, M.A. Abdu, P. Abadi, Z. Liu, L. Spogli, W. Wan, 2021. Challenges to equatorial plasma bubble and ionospheric scintillation short-term forecasting and future aspects in east and southeast Asia. Surveys in Geophysics, 42, 201–238.

Ma G., T. Maruyama, 2006. A super bubble detected by dense GPS network at east Asian longitudes. Geophysical Research Letters, 33(21), L21103. https://doi.org/10.1029/2006GL027512.

Mullen J.P., E. MacKenzie, S. Basu, H. Whitney, 1985. UHF/GHz scintillation observed at scension island from 1980 through 1982. Radio Sci., 20, 357–365. Doi: 10.1029/RS020i003p00357.

Nguyen Thanh D., M. Le Huy, C. Amory-Mazaudier, R. Fleury, S. Saito, T. Nguyen Chien, H. Pham Thi Thu, T. Le Truong, M. Nguyen Thi, 2021.

Characterization of ionospheric irregularities over Vietnam and adjacent region for the 2008-2018 period. Vietnam Journal of Earth Sciences, 43(4), 1–20. https://doi.org/10.15625/2615-9783/16502.

Perkins F., 1973. Spread F and ionospheric currents. J. Geophys. Res., 78, 218–226. Doi: 10.1029/JA078i001p00218.

Pi X., A.J. Mannucci, U.J. Lindqwister, C.M. Ho, 1997. Monitoring of global ionospheric irregularities using the worldwide GPS network. Geophys. Res. Lett., 24(18), 2283–2286.

Rodrigues F.S., E.R. de Paula, M.A. Abdu, A.C. Jardim, K.N. Iyer, P.M. Kintner, D.L. Hysell, 2004. Equatorial spread F irregularity characteristics over São Luís, Brazil, using VHF radar and GPS scintillation techniques, Radio Sci., 39, RS1S31. Doi: 10.1029/2002RS002826.

Saito S., T. Maruyama, 2006. Ionospheric height variations observed by ionosondes along magnetic meridian and plasma bubble onsets. Ann. Geophys., 24, 2991–2996. https://doi.org/10.5194/angeo-24-2991-2006.

Shiokawa K., C. Ihara, Y. Otsuka, T. Ogawa, 2003. Statistical study if nighttime medium-scale traveling ionospheric disturbances using midlatitude airglow images. J. Geophys. Res., 108(A1), 1052. Doi: 10.1029/ 2002JA009491.

Tran T.L., M. Le Huy, C. Amory-Mazaudier, R. Fleury, 2017. Climatology of ionospheric scintillation over the Vietnam low-latitude region for the period 2006–2014. Advances in Space Research, 60(8), 1657–1669.

Yang Z., Z. Liu, 2016. Correlation between ROTI and ionospheric scintillation indices using Hong Kong low-latitude GPS data. GPS Solutions, 20(4), 815–824. https://doi.org/10.1007/s10291-015-0492-y.

Yokoyama T., 2017. A review on the numerical simulation of equatorial plasma bubbles toward scintillation evaluation and forecasting. Progress in Earth and Planetary Science, 4(37), 1–13. Doi: 10.1186/s40645-017-0153-6.

Zhang Y., W. Wan, G. Li, L. Liu, L. Hu, B. Ning, 2015. A comparative study of GPS ionospheric scintillations and ionogram spread F over Sanya Y. Ann. Geophys., 33, 1421–1430.

Zuccheretti E, et al., 2003. The new AIS-INGV digital ionosonde. Annals of Geophysics, 46, 647–659. https://doi.org/10.4401/ag-4377.